SCRAMJET COMBUSTOR AND NOZZLE COMPUTATIONS

ICAS-92-3.4.2

Pradeep S. Kamath,
Analytical Services and Materials, Inc.,
and
Charles R. McClinton, NASA Langley Research Center,
Hampton, Virginia.

Abstract

A three-dimensional parametric study of a scramjet combustor and nozzle configuration at flight Mach numbers of 8, 10, 12, 16 and 20 is conducted using the SHIP3D PNS code. The code is calibrated with data from tests conducted at Mach 10 flight enthalpy on a similar combustor configuration. The performance parameters evaluated in the study are the mixing (combustion) efficiency, combustor loads, and thrust over the flight Mach number range. Using typical combustor entrance conditions for each flight Mach number, computations are performed at equivalence ratios (ER) of 0.5, 1.0, 1.5, 2.0, 3.0 and 4.0, and also at 0.0 (only air flow) for reference. The fuel injectors studied are ramps and slots. Fuel is injected axially from the base of the ramp on one wall (body) and from the slot on the opposite wall (cowl). In this configuration, slot injection not only provides better protection to the cowl from the ramp shock-induced heating, but also increases mixing. Each case with non-zero ER is also computed with only ramp injection for comparison. It is seen that film cooling increases the engine specific impulse by 400 seconds at Mach 8 and 100 seconds at Mach 16 and 20. The results show the following trends with an increase in flight Mach number: the mixing efficiency decreases by 0.2 as the flight Mach number increases from 8 to 12, and changes little for higher Mach numbers. The decrease in mixing is not an effect of compressibility. It is the result of a large (factor of 3) decrease in the fuel-to-air velocity ratio and residence time over the Mach number range. The study demonstrates the powerful computational strategy of using a modified, highly efficient PNS code and a non-kinetic chemistry model to compute high-speed, turbulent, reacting flow in scramjet combustors and nozzles.

1. Introduction

Hydrogen-fueled, air-breathing supersonic combustion ramjet (scramjet) engines are currently being developed for speeds up to Mach 25. These engines have been tested at conditions corresponding to flight speeds up to Mach 8 [1]. However, due to the limitations of the test facilities and instrumentation, there has been little testing at higher speed flight conditions. Thus computational fluid dynamics (CFD) codes play a critical role in the analysis of these engines for flight conditions beyond ground test capabilities.

CFD codes are currently being applied for diagnostic and performance evaluation of these high-speed scramjet flow paths. The SHIP3D PNS code is being used extensively for this purpose, because of its speed and its demonstrated capability to compute scramjet combustor and nozzle flow fields. The main content of this paper is one such parametric study conducted using the SHIP3D code. The objective of the study is to quantify the trends in some of the combustor performance parameters in the flight Mach number range from 8 to 20. The parameters chosen are the mixing (combustion) efficiency, wall heat flux and engine specific impulse. The combustor chosen for the study is similar in some respects to one tested at Mach 10 flight enthalpy. Data from those tests are used for code validation to support the results from this study.

2. Parametric Study

Figures 1(a) and 1(b) show the baseline geometry of the combustor-nozzle configuration analyzed in this parametric study. In Figure 1(a), the side view shows the fuel injectors, the ramp on the body side and the step on the cowl side. The computational domain was a section of width 2.54 cm (1"), shown in the plan and frontal views. Having symmetry planes as side boundaries simulated the effect of having several such sections on either side. The combustor entrance (gap) height was 5.08 cm and the combustor length was 60.16 cm (11.84 gap heights). The base of the ramp was at 2 gap heights and the step was at 2.25 gap heights from the entrance. The ramp angle was 9.648 degrees and there was no sweep. The ramp fuel injection orifice diameter was 0.508 cm and the slot height was 0.127 cm. These dimensions constituted the baseline configuration, and the only variations from it were changes in the ramp angle (7.407 and 11.68 degrees) and the sweep angle (5 and 10 degrees) to study their effect on mixing at Mach 16 flight conditions (see subsection 5.1). The overall length of the combustor-nozzle model was 140 cm and the cowl trailing edge was at 90 cm from the entrance (Figure 1(b)).

Table 1 presents the combustor entrance conditions and freestream conditions selected for the computations at different flight Mach numbers for a 95761 Pa (2000 psf) dynamic pressure trajectory. The flow entering the combustor was assumed to be uniform at the entrance conditions given in Table 1. The effect of the shocks and the boundary layer entering the combustor were neglected so as to better assess the mixing enhancement due to the ramps. The equivalence ratio (ER), defined as the ratio of the actual fuel mass flow rate to the fuel mass flow rate at stoichiometric conditions, was varied from 0.0 to 4.0. In the baseline configuration, all the fuel was injected parallel to the flow. Computations with injection angles of 10, 20 and 30 degrees were performed at Mach 16 flight conditions to study the effect on mixing. Ramp injection was at Mach 3 and slot injection was at Mach 2.5. Each case (ER) was also computed with all the fuel injected through the ramp. The fuel total temperature was fixed at 1000 degrees K and the fuel injection pressures for the ramp and slot were adjusted to get the desired fuel mass flow rates. The wall temperature was also 1000 degrees K.

3. Solution Methodology

The SHIP3D Parabolized Navier-Stokes (PNS) code, was used to perform all the computations. It is a vectorized and highly modified version [2] of the original SHIP code [3], with exponential (power-law) differencing and block-correction for convergence acceleration [4]. The discretized equations governing the transport of momentum, pressure-correction (continuity), energy, species and turbulence are solved one at a time, line-by-line with a tridiagonal matrix solver.

To adapt the SHIP3D PNS code to the configuration shown in Figure 1, which has base regions where the flow may be expected to recirculate, the following procedure was used. Marching was initiated at the combustor entrance, using the conditions given in Table 1 uniformly across the cross-section, on a 41x51 grid clustered at all the four boundaries. After traversing the first 2.54 cm, the computational domain was decomposed into two 21x51 blocks to accommodate the ramp and marching was continued for the next 7.62 cm, during which the blocks communicated with each other through patched boundary conditions. At the end of this transition section, the domain was reduced to one 41x101 block, the flow from the base of the ramp was patched on to the domain and marching was resumed. At the step, the flow from the base was picked up by patching and marching continued past the combustor exit to the cowl trailing edge, where the external flow at the freestream conditions was

patched above the engine flow. Marching was then continued to the exit of the nozzle. In the region downstream of the transition section, the smallest cell size was 5 microns next to the wall, resulting in a cell Reynolds number (y^+) of about 1.0, small enough for heat transfer calculations.

The configuration shown in Figure 1 has base regions where the flow can be expected to recirculate. Also, the flow can separate where the oblique ramp shock impinges on the cowl wall. The measures to be taken to prevent the space-marching solution from breaking down in these regions of locally elliptic flow are described in detail in reference [2]. In the base regions, it involves the axial injection of air from the portions of each base not covered by fuel injection ports [11]. The resulting gain in air mass is usually small (less than 0.1 percent) because of the low pressure (0.25 of entrance pressure) and velocity (0.01 of entrance velocity) of the injected air.

Hydrogen-air chemistry in the combustor was modelled with a one-step, non-kinetic, partial reaction model. This model requires the specification of a reaction efficiency, a parameter that determines the extent to which the one-step reaction of H2 and O2 to H2O is allowed to proceed to completion. Thus, the combustion efficiency is the product of the mixing and reaction efficiencies,

$$\eta_c = \eta_m \eta_r$$

The reaction efficiency used in the study was 0.8. The choice is based on previous calculations (unpublished) which showed that this value predicts the same heat release as that from a full equilibrium reaction mechanism [5].

A high-Reynolds number q-ω closure model [6] was used to treat turbulence. In this model, a compressibility correction based on compressible dissipation, proposed in [7] and adapted to a two-equation model in [8], has been implemented. This correction, designed to simulate the inhibiting effect of compressibility on turbulence, has been shown to reproduce the reduction in the growth rate of a compressible turbulent shear layer with convective Mach number. The observed effect of the correction in the present study is discussed in subsection 5.1.

4. SHIP3D Code Validation

This section presents comparisons of the SHIP3D PNS code with the SPARK3D elliptic code and with experimental data. These comparisons are included to support the computational results presented in this paper.

4.1 Comparison With an Elliptic Calculation

The parabolic solution methodology used in SHIP3D to simulate the ramp injector flow field is first compared to a SPARK3D elliptic computation. It should be noted that the two calculations differ not just in the (parabolic or elliptic) governing equations solved but also in the turbulence models used. In the SHIP3D computation, a two-equation model [6] with a turbulent Schmidt number of 0.9 was used. The SPARK3D code has the (zero-equation) Baldwin-Lomax model [10], and the turbulent Schmidt number was set to 0.5 in accordance with previous validation studies [14]. The test case, shown in Figure 2, involves injection from a single, unswept, 10 degree ramp into a Mach 2 air stream in a rectangular duct. The injection angle is 10 degrees into the flow. The ramp introduces a swirl into the flow by compressing and thus pushing it around the sides. This swirling flow distorts the circular cross-section of the jet injected from the base into a kidney shape. Figure 2 shows the injectant contours at a distance of nine ramp heights downstream of injection for both the SHIP3D PNS and SPARK3D elliptic computations. Most of the features of the jet are the same in the two calculations, implying that those flow features not reproduced in the PNS computation, such as the recirculation region near the base of the ramp, had only a small influence on mixing. These results demonstrate that the SHIP3D code and solution methodology described in the previous section produce high-quality engineering results for these configurations involving ramp injection. Similar validation for slot injection is documented in references [11,12].

4.2 Comparison With Experimental Data

The experimental data considered here was obtained on a model scramjet combustor tested by GASL in the Calspan 96-inch shock tunnel [13]. The conditions simulated in those tests are close to those expected at Mach 10 flight at a dynamic pressure of 1000 psf 47880 Pa (1000 psf). The combustor model, shown schematically in Figure 3(a) was a duct of rectangular cross-section, with an entrance gap height of 5.08 cm (2 inches), a width of 35.56 cm (14 inches) and a length of 101.6 cm (40 inches). The combustor entrance pressure, temperature and Mach number were 37921 Pa, 1073 degrees K and 3.97 respectively. Hydrogen fuel was injected at an angle of 10 degrees to the combustor wall from seven wall-mounted ramps on the "body" (bottom wall) side. The ramp angle was 10.3 degrees and the sweep angle was 10 degrees. There was no slot fuel injection at the step. The bottom (body) and top (cowl) walls were instrumented with static pressure taps and heat flux gages. In-stream measurements included pitot pressures at the combustor entrance and exit planes.

In the computations, the spanwise extent of the computational domain was half the distance between two adjacent ramps and included half of one ramp. Having symmetry planes for side boundaries simulated the effect of having the computational domain near the center of the duct with a number of similar sections on either side. Fuel injection was at Mach 1.67 at a pressure that provided an ER of 0.99. The top and bottom boundaries of the computational domain were isothermal walls at ambient temperature (292 degrees K), the same as the fuel total temperature.

Figures 3(a) and 3(b) show the normalized heat flux and pressure on the cowl as functions of distance from the combustor entrance. These figures show good agreement between the measurements and computations. The peaks seen in these figures occur at the same axial locations for the heat flux and pressure and were shock-induced. The oblique shock generated by the ramp protruding from the body wall into the supersonic flow impinged on the cowl wall at 20 cm., causing the first peak. Each subsequent peak on the cowl was caused by the same shock after reflection from the body wall. This is confirmed by the body-side curves (not included here) which show peaks and valleys that are shifted axially from those on the cowl side. In Figure 3(b), the computation does show some lateral variation near the cowl step, but there were few measurements there to confirm that trend. Superimposed on the effect of shocks in Figures 3(a) and 3(b) is the upward trend in the average values due to combustion. The mixing and combustion efficiencies are discussed in the two following paragraphs.

Figure 3(c) shows the computed mixing efficiency along the length of the combustor. The mixing efficiency at a streamwise cross-section is the ratio of the fuel mass at that cross-section that can react completely (to the extent that it has mixed) to the fuel mass required to consume all the available oxygen (for a fuel-rich mixture) or the fuel itself (for a fuel-lean mixture). According to this definition, a fully mixed condition would have a mixing efficiency of unity for both fuel-rich and fuel-lean mixtures. Figure 3(c) shows three cases, two of which were not tested. For the swept ramp case, which was the geometry tested, the computed mixing efficiency at the exit is 0.75. The other two cases in Figure 3(b), one without sweep and one with equal ramp and slot injection, are presented to illustrate some interesting high-speed mixing characteristics which are relevant to the parametric study. Comparing the mixing for the unswept case with the swept ramp case, it is seen that the sweep accelerated mixing close to the injector. This observation is in accordance with previous studies [14]. But the swept ramp shows slower

mixing in the far-field than the unswept ramp which produced a sustained, linear increase in mixing. This indicates that to achieve a certain degree of mixing, a shorter combustor length suffices if sweep is included in the ramp. The oblique ramp shock is another feature of this flow that can improve mixing. This is demonstrated by the third curve in Figure 3(c), which is for equal ramp and slot injection. This curve shows an additional, intermittent acceleration in mixing. That this mixing enhancement occurred at the points of shock impingement on the cowl can be verified by comparing Figure 3(c) with Figure 3(a) or 3(b). The mixing efficiency at the exit of 0.88, which is about 0.13 higher than that for the other two cases, reflects enhanced mixing due to the impingement of the ramp shock on the wall jet of fuel from the slot. These results are relevant to the discussion in subsection 5.1.

When treating the hydrogen-air chemistry in these computations, it was found that setting the reaction efficiency to 0.8 (the value at Mach 10 for chemical equilibrium, as described in the second-to-last paragraph of Section 3) provided too much heat to the flow, resulting in wall pressures and heat fluxes that were too high compared to the measurements. This is attributed to the relatively low fuel and wall temperatures in the test. But in the parametric study, the fuel and wall temperatures were both fixed at 1000 degrees K. Thus a reaction efficiency of 0.8 was a more reasonable choice for the study.

The results presented in this subsection demonstrate the capability of the SHIP3D code to compute turbulent, reacting flow and heat transfer in scramjet combustors. It is a powerful tool for the analysis of scramjet combustor test results. The typical run time is one to two hours on a Cray YMP. Thus the code is also well-suited to conduct extensive parametric studies, where a large number (hundreds) of runs may be required to cover the entire parameter space.

5. Results of Parametric Study

The results of the parametric study are presented in Figures 4 through 14. The figures labeled (a) show the results for cases with equal ramp and slot fuel mass flow rates (hereafter referred to as ramp-slot injection) and the ones labeled (b) are for cases in which all the fuel was injected through the ramps (ramp injection). In most of the figures, the abscissa is ER, ranging from 0.0 to 4.0, and each curve is for one flight Mach number. In these figures, the ER is denoted by the symbol ϕ. Plotted as ordinates are the parameters of interest in this study. The results for each set of parameters are discussed in the following subsections.

5.1 Mixing

Figures 4(a) and 4(b) show the mixing efficiency at the exit of the combustor for ramp-slot injection and for ramp injection. All the curves have a trough at an ER of 1.0, which is to be expected because stoichiometric proportions of fuel and air have to mix until the composition is uniform. The trend of particular interest is the decrease in mixing with flight Mach number in the range 8 to 12, as shown in Figure 5. The upper curve in Figure 5 shows that there was a drop of about 0.2 (30 percent) in the mixing efficiency between Mach 8 and Mach 12, with little further variation at higher Mach numbers. Such a drop in mixing with an increase in Mach number is normally attributed to the inhibiting effect of compressibility on turbulence. But that explanation is not applicable here because the correction designed to account for this effect [7,8] was not used in the turbulence model when performing these computations (the upper curve in Figure 5). However, the correction had only a small effect, as seen by comparing the two curves in Figure 5. This implies that the turbulent Mach number, which determines the magnitude of the correction, was small in this high-temperature flow field, although the convective Mach number [1] ranged from 0.1 at Mach 20 to 1.7 at Mach 8, high enough to have caused a significant reduction in the shear layer growth rate. The fact that both curves in Figure 5 follow the same trend and differ little indicates that the inhibiting effect of compressibility on shear layer growth rate was small in these flows. The larger drop in mixing with flight Mach number shown in Figure 5 is believed to be due to the large (factor of 3) decrease in the fuel-to-air velocity ratio and residence time in the combustor over the Mach number range [15]. These effects have been discussed in further detail in reference [16].

Another interesting trend is the effect of slot injection on mixing, seen by comparing Figures 4(a) and 4(b). One expects that slot injection, usually used for film cooling, would result in a decrease in the mixing efficiency because it involves fuel injection adjacent to the wall. That is indeed true for slot injection in a flow field devoid of shocks, as in a straight or diverging duct. But in the present configuration, the oblique shock produced by the ramp impinged on the cowl just downstream of the slot. This merging of the shocked air stream with the wall jet produced high rates of strain, thus generating turbulence and enhancing mixing. Also, ramp-slot injection produced a more uniform fuel distribution in the duct at the injection station. The higher mixing efficiency in Figure 4(a) when compared to that in Figure 4(b) is a manifestation of these effects. The effect of an impinging shock on a wall jet has been demonstrated both experimentally and computationally (also see Figure 3(c)) in film cooling studies involving shock impingement [9], where the effective cooling length of the film was seen to decrease drastically downstream of shock impingement due to enhanced mixing. The next subsection includes a discussion of the cooling effectiveness of slot injection in the presence of the ramp shock.

The effect of injection angle, ramp angle, and sweep angle on mixing are now discussed. These parametrics were conducted at the Mach 16 flight condition only. The effect of angular injection from the ramp on mixing is shown in Figure 6. Recall that in all the cases shown in Figures 4(a) and 4(b), the fuel was injected parallel to the duct walls. The case considered in Figure 6 is the 1.5 ER run at Mach 16 with ramp-slot injection. The fuel injection angles for these cases were 0, 10, 20, and 30 degrees up into the flow from the base of the 9.648 degree ramp. The results demonstrate the strong effect of injection angle on mixing, indicating that the mixing efficiencies in Figures 4(a) and 4(b) could have been improved by about 30 percent by going to a higher injection angle.

Next, the effect on mixing of increasing the ramp angle is discussed. Figure 7 shows the variation in the mixing efficiency for ramp angles of 7.407, 9.648 (baseline) and 11.86 degrees. An increase in the ramp angle can be expected to increase mixing in two ways: by inducing more swirl into the flow which would enhance mixing of the fuel injected from the ramp, and by generating a stronger shock that would enhance mixing of the fuel injected from the slot. In the second effect, oblique shock impingement on the wall jet produces high strain rates and generates turbulence, whereas its effect on the ramp jet is simply to deflect it slightly. The magnitude of the first effect is shown in the lower curve in Figure 7, which is for ramp injection. This curve shows that an increase in the ramp angle from 7.407 to 11.860 increased the mixing efficiency by 0.066. But the upper curve, which is for ramp-slot injection, shows three times as much increase in mixing for the same increase in the ramp angle. Thus, for this curve, it can be inferred that two-thirds of the increase in mixing was because of the effect of the stronger shock on the slot flow and only one-third was due to more swirl.

The third parameter of interest in mixing enhancement is the sweep angle. Swept ramps have been shown to generate more swirl and give better mixing than unswept ramps [14]. Figure 8 shows that when the sweep angle was increased from the baseline value of 0 to 5 degrees, the mixing efficiency increased by 0.013. But a 10 degree sweep increased the mixing by 0.129, indicating the strong sensitivity of mixing to sweep in this range of sweep angles, probably because the sweep angle was close to the Mach angle, which in this case, is 11 degrees.

5.2 Heat Transfer

The heat flux distribution on the body and cowl walls of the GASL combustor was discussed in subsection 4.2. In that case, the oblique shock generated by the ramp was reflected repeatedly between the body and cowl, producing peaks and valleys in the wall heat flux and pressure. Also, combustion produced higher peaks and higher valleys with axial distance. The flow field in the parametric combustor, which was similar in geometry to the GASL combustor, had many of the same features, with some variations over the ranges of Mach number and ER. Figures 9 through 13 show the heat flux results from the parametric study. The average heat flux on the body and the cowl are shown in Figures 9 and 10 and the peak values in Figures 11 and 12. Figure 13 shows the variation of the overall (body and cowl) average heat flux with the average wall pressure to illustrate that the combustor wall heat flux is governed more by fuel distribution (three-dimensional effects) than by wall pressure. These results are discussed in the following paragraphs.

Figures 9(a) and 9(b) show the average heat flux on the body side for ramp-slot and ramp injection cases respectively. Note that at low Mach numbers, the heat load increases slightly with ER in the lower range of ERs. But at higher ERs, and at higher Mach numbers, the average heat flux on the body side decreases with an increase in ER. This body-side cooling effect is stronger for ramp injection (Figure 9(b)) where more unburned fuel next to the wall acted as a coolant, and at an ER of 4.0, completely insulated the wall. In both figures, this cooling effect is most evident at high Mach numbers where the temperature difference between the fuel and air streams was the largest.

Figures 10(a) and 10(b) show the average heat flux on the cowl side. Figure 10(a) shows that for ramp-slot injection, the wall heat flux decreased as the total (and slot) ER was increased. Figure 10(a) also shows the strong effect of slot injection on the cowl wall heat flux at Mach 20 and 16. At lower Mach numbers, slot cooling was less effective because of faster mixing (see Figure 5) and a higher pressure gradient in the combustor [15]. For all-ramp injection (Figure 10(b)), the cowl-side average heat flux actually increased slightly with ER because, without slot injection, there was little if any unburned fuel next to the cowl wall to provide cooling, while shock-induced heating on the cowl was enhanced by a combustion-induced increase in the wall pressure.

The peak heat flux on the body wall is shown in Figures 11(a) and 11(b). In these figures, the number shown near each symbol (peak value) indicates the location of that peak from the combustor entrance in cm. First consider the Mach 12, 16, and 20 curves in these figures. At these Mach numbers, the peak on the body occurs where the ramp shock, after being reflected from the cowl, first impinges on the body. Both figures show that with increasing Mach number, the peak increased in magnitude and its location moved downstream. This is as expected because the oblique ramp shock-induced pressure rise increases, and the shock angle decreases as the Mach number increases. At the lower Mach numbers (see the Mach 8 and Mach 10 curves), the peak locations show a stronger dependence on ER because the flow field was less dominated by shocks, and combustion had a greater influence on the peak location.

Next, consider Figure 12(a), which shows the peak heat flux on the cowl for ramp-slot injection. In this figure, the peak locations are shown only for the Mach 16 and 20 curves due to limited space. When compared with Figure 12(b), Figure 12(a) shows the large extent of local cooling that the film provided at high Mach numbers. The film, when injected on the cowl slightly upstream of impingement of the ramp shock, served as a thermal cushion against intense, local, shock-induced heating. The cooling effect of the film was only local because the shock quickly disperses the film by enhancing its otherwise slow mixing rate. Thus local cooling and better mixing were simultaneously achieved with slot injection. At higher (slot) ERs, slot injection effectively pushed the peak location to the exit of the combustor, as seen from the numbers above the Mach 16 and 20 curves in Figure 12(a). These peaks near the combustor exit, caused by the ramp shock arriving at the cowl after multiple reflections, were enhanced by combustion of the slot fuel adjacent to the cowl wall at these high ERs and are higher than those at the first shock impingement location. For ramp injection (Figure 12(b)), the cowl was largely unprotected from the ramp shock. Thus, the peak location was always at the first shock impingement point on the cowl and the magnitude changed little with ER for each Mach number.

Figure 13 presents the normalized combustor wall heat load (average wall heat flux) versus normalized combustor average wall pressure. This figure shows that over a large range of ER and Mach number, the average wall (body and cowl) heat flux decreased even though the average wall pressure increased with increasing ER. This implies that the net effect of the injected fuel (from a thermal loads aspect) was to cool the walls. To understand this trend, it should be noted that heat transfer to the wall is a local effect, driven by the local temperature gradient and pressure, and is thus lowered by the presence of unreacted fuel next to the wall. Also included in Figure 13 is the curve showing the expected trend in a hypersonic flow of a single (air) stream, where experimental data has shown that the heat flux is proportional to pressure to the power of 0.85 [17]. Note that for Mach 8 at low ER, this trend is reproduced. However, at higher Mach numbers this trend is reversed. Clearly, the main reason for the decrease in heat flux with an increase in pressure was the large (total) temperature decrease resulting from the high fuel concentrations adjacent to the wall. This effect even neutralized the combustion-induced heating.

5.3 Specific Impulse

The net thrust produced by the combustor-nozzle model is the algebraic sum of three terms: 1) the net wall pressure integral, 2) the fuel stream thrust $\left[\left(p+\rho w^2\right)A\right]_{fuel}$ and 3) the skin friction drag. One method of evaluating the combustor performance is by an incremental specific impulse (in seconds),

$$\Delta I_{sp} = 0.10204\left(\frac{T_\phi - T_{\phi=0}}{\dot{m}_{fuel}}\right)$$

which is positive since the net thrust for a case with fuel exceeds that for the case without fuel at the same combustor entrance conditions (flight Mach number). The steep decline in the specific impulse with Mach number is attributable to three reasons: 1) lower pressure rise in the combustor [15], 2) lower mixing efficiency (Figure 5),and 3) higher frictional drag. The specific impulse was higher with slot injection because of both better mixing (Figures 4(a) and 4(b)) and lower skin friction. The two curves in Figure 14 indicate that film cooling increased the engine specific impulse by 400 seconds at Mach 8 and approximately 100 seconds at Mach 16 and 20.

6. Summary

This paper described a three-dimensional parametric study of a scramjet combustor-nozzle configuration in the flight Mach number range of 8 to 20. The computations were performed with the SHIP3D PNS code. This code was calibrated with data from tests conducted at Mach 10 flight enthalpy on a similar combustor configuration. The study demonstrated the powerful computational strategy of using a highly efficient, modified PNS code and a non-kinetic chemistry model to analyze test data and conduct parametric studies of scramjet combustors and nozzles.

The results of the parametric study are summarized as follows:

1) The mixing efficiency decreased by 0.2 when the flight Mach number increased from 8 to 12 and showed little change at higher Mach numbers. The drop in mixing was caused, not by a compressibility-induced reduction in shear layer growth

rate, but by a large (factor of 3) decrease in the fuel-to-air velocity ratio and the residence time in the combustor. At an ER of 1.5, a typical operating condition, the mixing efficiency, with ramp-slot injection, achieved over a length of 10 entrance gap heights decreased from 0.68 to 0.48 over the flight Mach number range. For ramp injection, the mixing efficiencies were lower than ramp-slot injection by 0.2 to 0.3.

2) The protruding ramp injector generated an oblique shock that impinged on the cowl. Ramp-slot injection produced better mixing, both because of the interaction of this shock with the slot fuel, and because of better fuel distribution in the duct. The former effect was enhanced when the ramp angle was increased. Mixing was also enhanced when the ramp fuel injection angle and sweep angle were increased.

3) The impingement of the ramp shock on the cowl caused a hot spot at that location. This was mitigated by slot injection on the cowl, which lowered the peak heat flux by 50 percent at Mach 16 and by as much as 75 percent at Mach 20. At lower Mach numbers, slot injection was generally less effective because of faster mixing and larger combustion-induced pressure gradients. However, fuel injection adjacent to any wall, either through the ramp or the slot had a cooling effect, particularly at the higher Mach numbers, because of the large temperature difference between the fuel and the air streams.

4) Net thrust was generated in all the cases with non-zero ER. Comparison of ramp-slot injection with ramp injection showed an increase in the incremental specific impulse of 400 seconds at Mach 8 and 100 seconds at Mach 16 and 20 for ramp-slot injection, because of higher mixing and lower frictional drag.

References

1. Northam,G.B. and Anderson,G.Y.: "Supersonic Combustion Ramjet Research at Langley," AIAA Paper No. 86-0159, 1986.
2. Kamath, P.S., Mao,M. and McClinton,C.R.: "Scramjet Combustor Analysis With the SHIP3D PNS Code," AIAA Paper No. 91-5090, 1991.
3. Markatos,N.C., Spalding,D.B. and Tatchell,D.G., "Combustion of Hydrogen Injected into a Supersonic Airstream (The SHIP Computer Program)," NASA CR-2802, April 1977.
4. Patankar,S.V., "A Calculation Procedure for Two-Dimensional Elliptic Situations," Numerical Heat Transfer, v 4, 409-425, 1981.
5. Jachimowski,C.J.: "An Analytical Study of the Hydrogen-Air Reaction Mechanism With Application to Scramjet Combustion," NASA TP 2791, February 1988.
6. Coakley,T.J., "Turbulence Modeling Methods for the Compressible Navier-Stokes Equations," AIAA Paper 83-1693, 1983.
7. Sarkar,S., Erlebacher,G., Hussaini,M.Y. and Kreiss,H.O.: "The Analysis and Modelling of Dilatational Terms in Compressible Turbulence," J Fluid Mechanics, v 227, p 473-493, 1991.
8. Narayan,J.R. and Sekar,B., "Computation of Turbulent High Speed Mixing Layers Using a Two-Equation Turbulence Model," presented at the Computational Fluid Dynamics Symposium on Aeropropulsion, NASA Lewis Research Center, April 24-26, 1990.
9. Kamath,P.S., Holden,M.S., McClinton,C.R.: "Experimental and Computational Study of the Effect of Shocks on Film Cooling Effectiveness in Scramjet Combustors," AIAA Paper No. 90-1713, 1990.
10. Baldwin,B.S. and Lomax,H., "Thin Layer Approximation and Algebraic Model for Separated Turbulent Flows," AIAA Paper 78-257, 1978.
11. Kamath,P.S., Hawkins,R.W., Baker,N.R. and McClinton,C.R., "A Highly Efficient Engineering Tool for Three-Dimensional Scramjet Flow Field and Heat Transfer Computations," presented at the Computational Fluid Dynamics Symposium on Aeropropulsion, NASA Lewis Research Center, April 24-26, 1990.
12. Kamath,P.S., Baker,N.R. and McClinton,C.R.: "A Computational Design Tool for Scramjet Combustor Film Cooling and Fuel Mixing Predictions," AIAA Paper No. 90-0645, 1990.
13. Orth,R.C., Torrillo,D., Rizkalla,O.F., Lempert,O.F. and Erdos,J.I., "Results of Parametric Scramjet Combustor Experiments Conducted in the Calspan Shock Tunnel - 4th Entry," GASL TR 329, Volumes 1 and 2, February 1991.
14. Riggins,D.W. and McClinton,C.R., "A Computational Investigation of Flow Losses in a Supersonic Combustor," AIAA Paper 90-2093, 1990.
15. Kamath,P.S., Mao,M. and McClinton,C.R.: "A Parametric Study of Scramjet Combustors for Mach 8 to Mach 20 Flight," AIAA Paper No. 91-1412, 1991.
16. Riggins,D. and McClinton,C.R.: "A Computational Investigation of Mixing and Reacting Flows in a Supersonic Combustor," AIAA Paper No. 92-0626, 1992.
17. Holden,M.S.: "Shock Wave - Turbulent Boundary Layer Interaction in Hypersonic Flow," AIAA Paper No. 77-45, 1977.

TABLE 1. CONDITIONS AT COMBUSTOR ENTRANCE AND IN FREESTREAM

Flight Mach Number	Combustor Entrance Conditions				Freestream Conditions	
	P,Pa	W, m/sec	T°K	M	P_∞,Pa	T_∞,°K
8	120,200	2059	1030	3.20	2137	223
10	129,800	2721	1211	3.90	1368	226
12	125,300	3333	1428	4.40	950	228
16	124,106	4678	2135	5.05	534	238
20	319,360	5789	2957	5.31	342	247

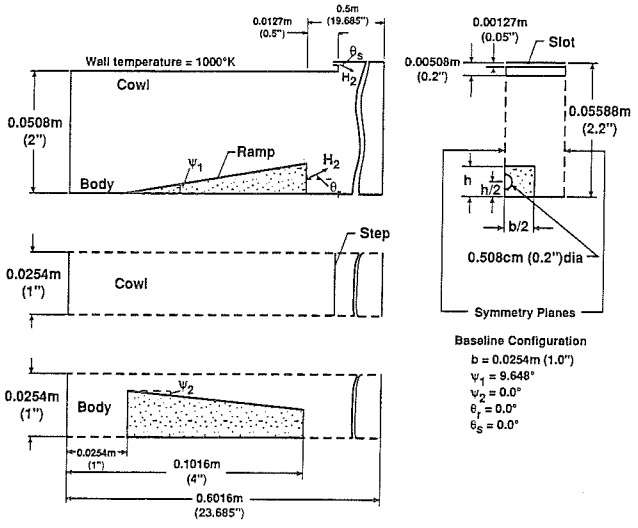

Figure 1a. Geometry of Parametric Combustor

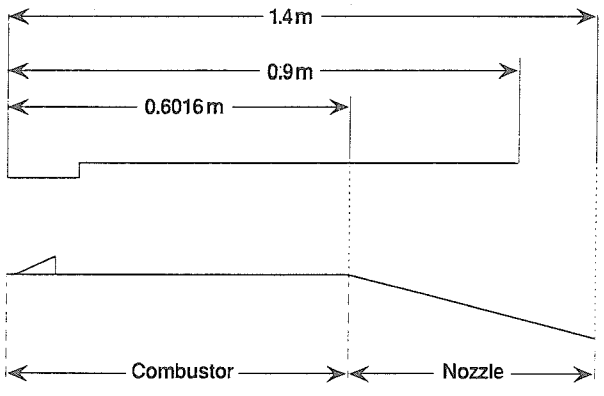

Figure 1b. Combustor and Nozzle Geometry

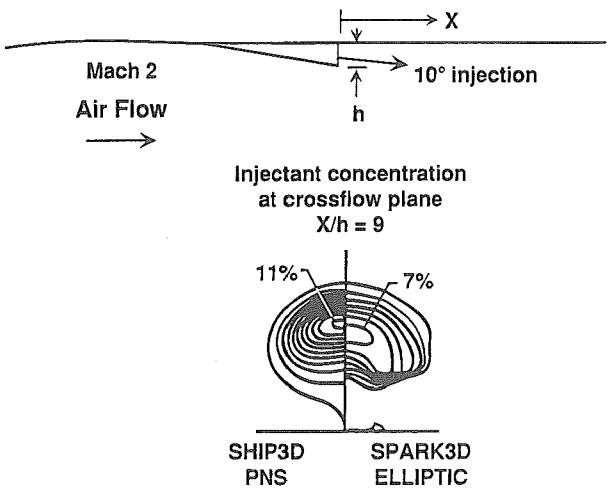

Figure 2. SHIP-SPARK Comparison for Ramp Injection

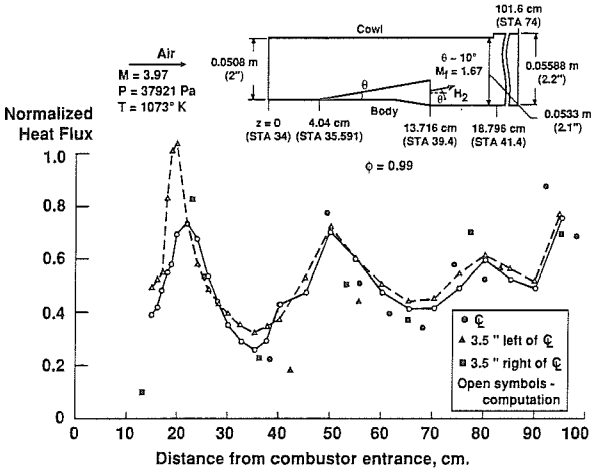

Figure 3a. Cowl-Side Heat Flux for GASL Combustor

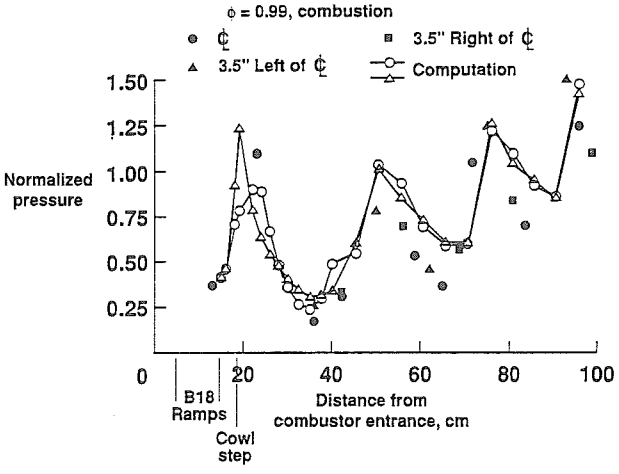

Figure 3b. Cowl-Side Pressure for GASL Combustor

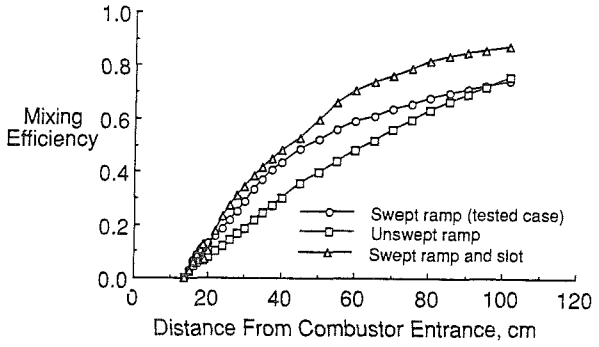

Figure 3c. Computed Mixing for GASL Combustor

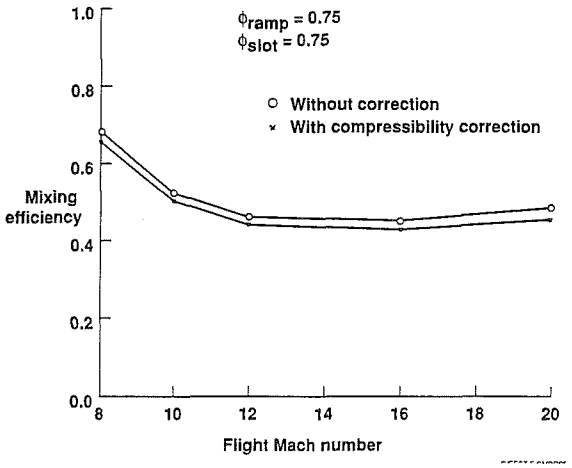

Figure 5. Effect of Compressibility on Mixing

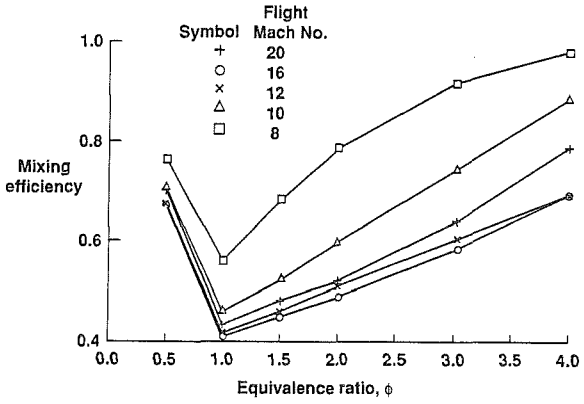

Figure 4a. Mixing for Ramp and Slot Injection

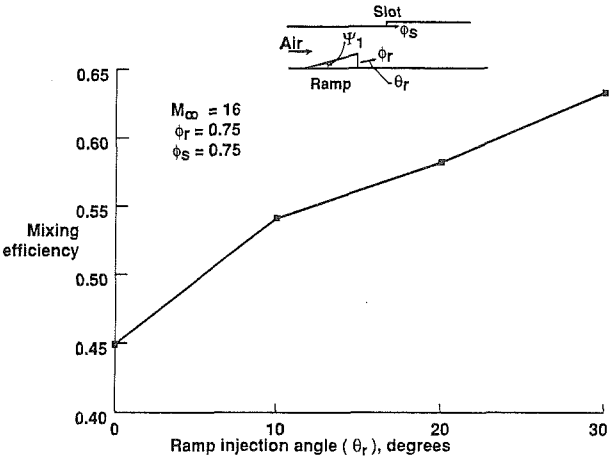

Figure 6. Effect of Ramp Injection Angle on Mixing

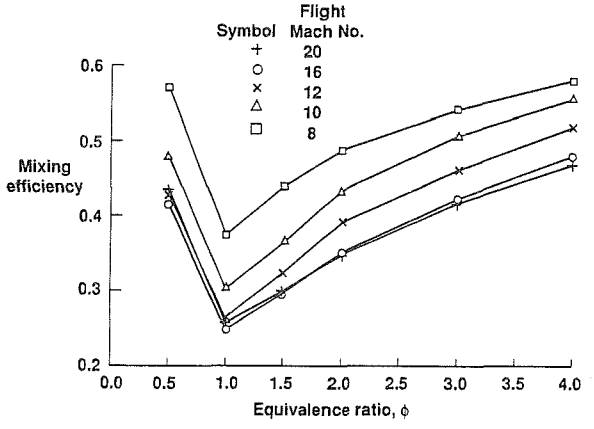

Figure 4b. Mixing for Ramp Injection

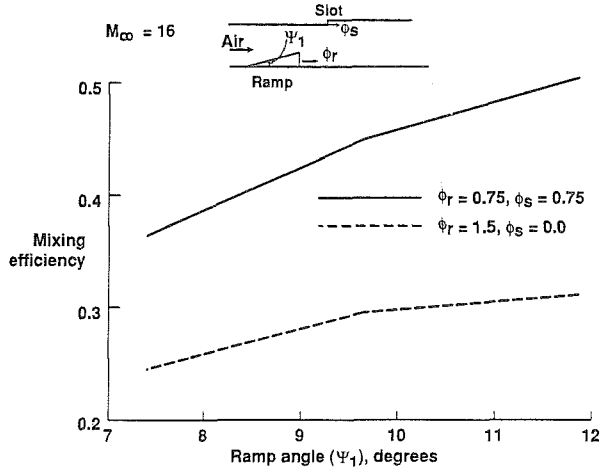

Figure 7. Effect of Ramp Angle on Mixing

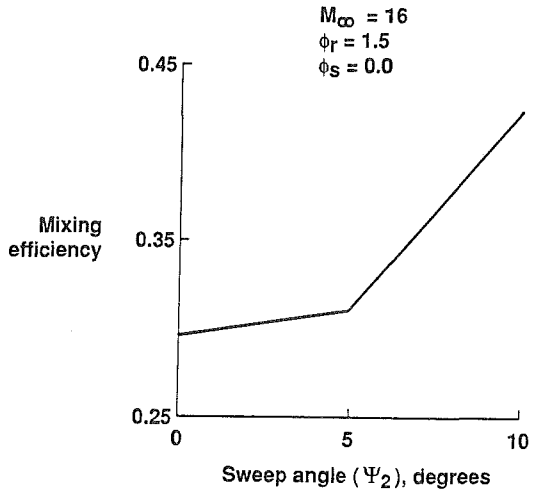

Figure 8. Effect of Sweep Angle on Mixing

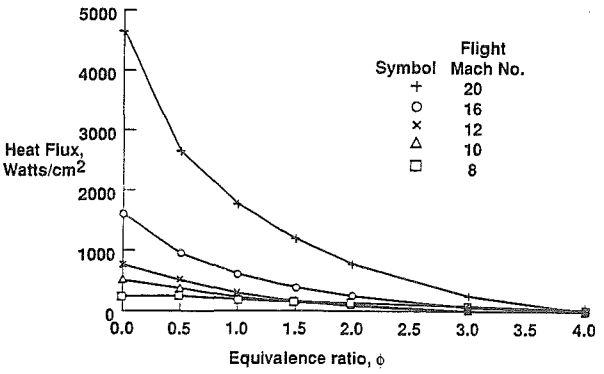

Figure 10a. Cowl Average Heat Flux for Ramp-Slot Injection

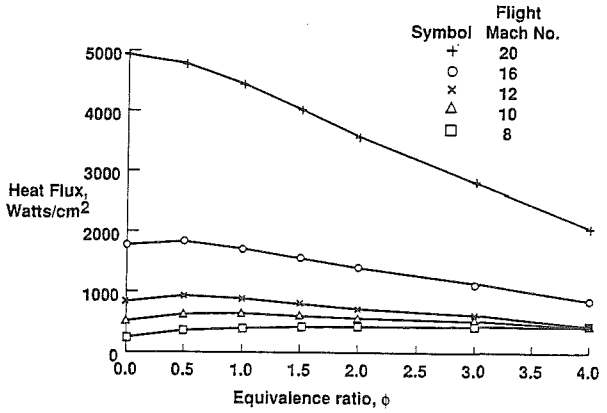

Figure 9a. Body Average Heat Flux for Ramp-Slot Injection

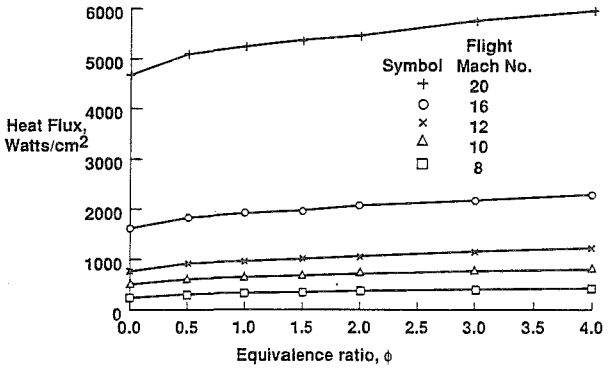

Figure 10b. Cowl Average Heat Flux for Ramp Injection

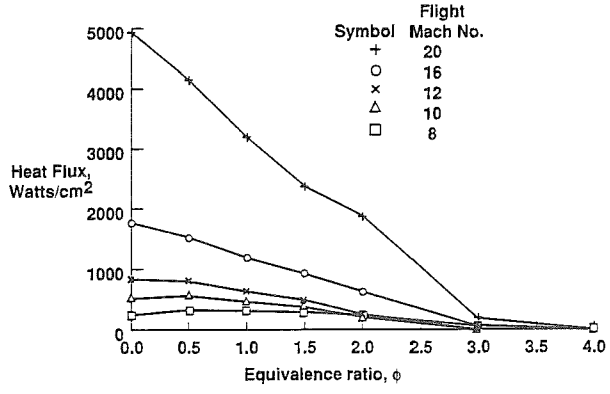

Figure 9b. Body Average Heat Flux for Ramp Injection

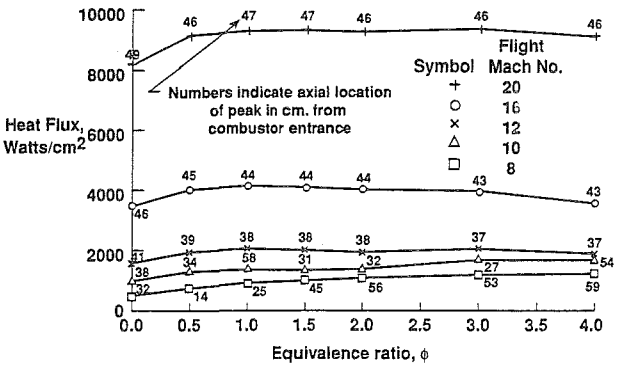

Figure 11a. Body Peak Heat Flux for Ramp-Slot Injection

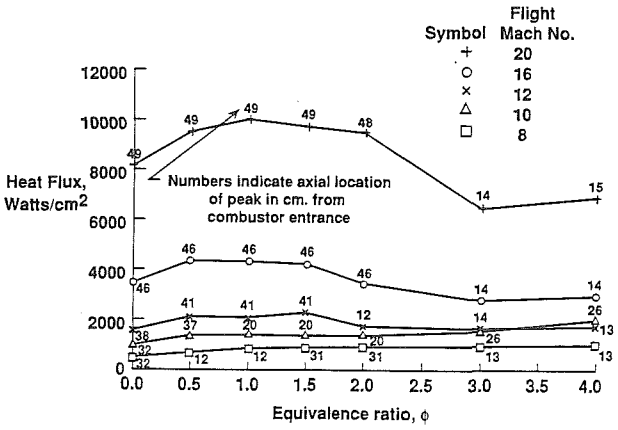

Figure 11b. Body Peak Heat Flux for Ramp Injection

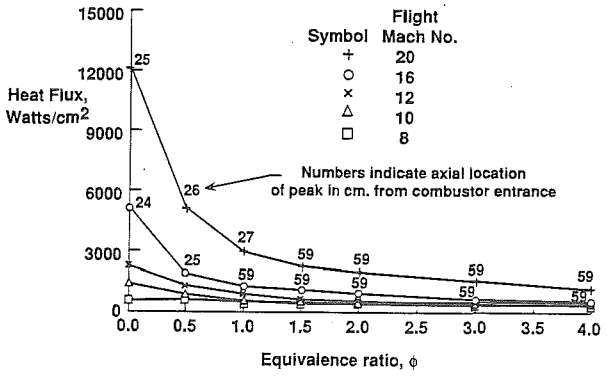

Figure 12a. Cowl Peak Heat Flux for Ramp-Slot Injection

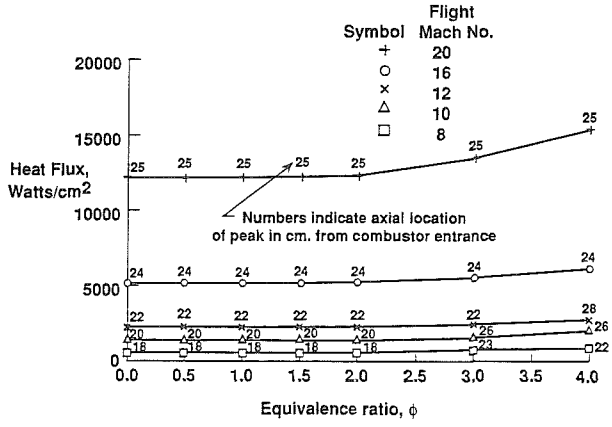

Figure 12b. Cowl Peak Heat Flux for Ramp Injection

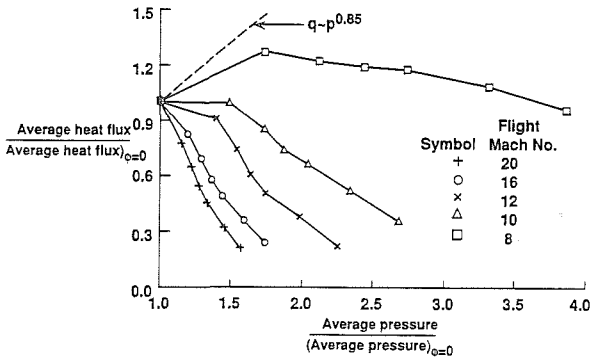

Figure 13. Wall Heat Flux vs Wall Pressure for Ramp-Slot Injection

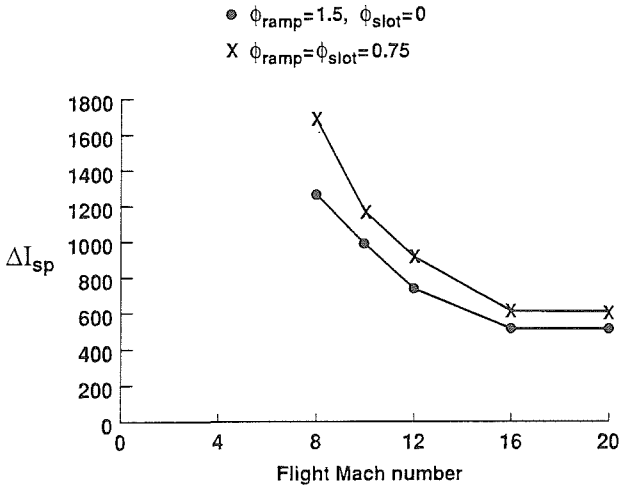

Figure 14. Incremental Specific Impulse vs Flight Mach Number